JACS
JOURNAL OF THE AMERICAN CHEMICAL SOCIETY
pubs.acs.org/JACS
Article

Tuning Supramolecular Polymer Assembly through Stereoelectronic Interactions

Will R. Henderson, Guancen Liu, Khalil A. Abboud, and Ronald K. Castellano*

Cite This: https://doi.org/10.1021/jacs.1c05522
Read Online
ACCESS | Metrics & More | Article Recommendations | Supporting Information

ABSTRACT: The supramolecular polymerization of 2,11-dithia[3.3]paracyclophanes through self-complementary intermolecular and transannular amide hydrogen bonding is presented. An $n \rightarrow \pi^*$ interaction between the amide hydrogen bonding units and the central bridging atom results from the single-point exchange of a carbon atom for a sulfur atom. This orbital donor–acceptor interaction can be strengthened by oxidizing the sulfide to a sulfone which acts to shorten the donor···acceptor distance and increase orbital overlap. Experimental signatures of the increased $n \rightarrow \pi^*$ interaction include larger isodesmic polymerization elongation constants in solution, changes in characteristic bond stretching frequencies, and geometric/structural changes evaluated by X-ray crystallography. The experimental data are supported by extensive computational investigations of both assembling and nonassembling 2,11-dithia[3.3]paracyclophanes as well as a rationally designed model system to confirm the role of stereoelectronic effects on supramolecular polymer assembly.

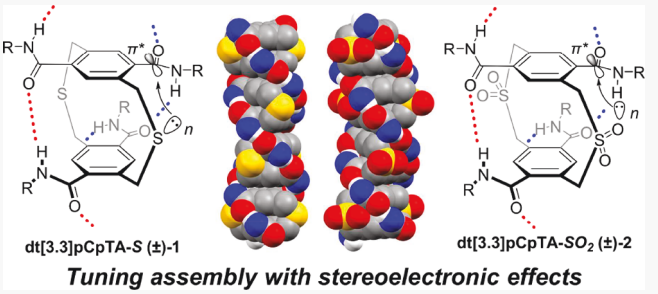

INTRODUCTION

Supramolecular polymers are a class of macromolecules formed by directional, reversible noncovalent interactions between monomers that result in polymeric properties in the bulk and in solution.[1−8] To overcome entropically unfavorable intermolecular association, a thermodynamic driving force comes in the form of enthalpically favorable hydrogen bonding, $\pi-\pi$ interactions, metal coordination, or halogen bonding. An acute thermodynamic balancing act underpins the achievement of large degrees of polymerization. The ability to tune supramolecular assembly strength through electronic and structural changes of the monomer without changing the overall supramolecular structure is essential for establishing structure–property relationships that will allow the design of new functional supramolecular polymers.

Pioneering recent work by Raines,[9] Weinhold,[10] and Alabugin[11] has allowed the rationalization of observable physical properties such as conformational bias or bond strength on the basis of stereoelectronic interactions. Over the last 20 years, it has been appreciated that certain stereoelectronic interactions, such as the $n \rightarrow \pi^*$ interaction, can act to stabilize the folded states of polypeptides[12−15] and modulate the reduction potentials of strained disulfide bonds in natural products.[16] Moreover, intramolecular stereoelectronic interactions, as we showed years ago using 1-aza-adamantanetrione donor–σ–acceptor molecules, can serve as a significant driving force for intermolecular self-assembly.[17−21] Herein, we present an example of an intramolecular $n \rightarrow \pi^*$ interaction which acts as a secondary effect to alter the assembly strength of an intermolecularly hydrogen bonded supramolecular polymer.

Recently, our group introduced the class of supramolecular polymers based on self-assembly of [n.n]paracyclophanes ([**n.n**]**pCps**, n = 2, or 3) promoted by transannular and intermolecular hydrogen bonding.[22−26] The stereochemistry of these supramolecular assemblies is also of fundamental interest as all assemblies of [**n.n**]**pCps** have been homochiral in the solid-state due to their fixed planar-chirality at the monomer.[27] Two recent examples of heterochiral supramolecular polymers further demonstrate the fundamental change in assembly stereochemistry when chirality is established in this way.[28,29] Self-assembling [**n.n**]**pCps** with four equivalent amide hydrogen bonding units ([**n.n**]**pCpTAs**) have been shown to assemble via an isodesmic (equal-K) mechanism by pathway selection of the *anti*-conformer.[24] We have shown that a combination of intermolecular H-bonding, $\pi-\pi$ distances, and monomer dynamics is responsible for dictating the self-complementary association of these molecules with an elongation constant K_{el} spanning 3 orders of magnitude in $CDCl_3$ (from 20–5000 M^{-1}) despite the presence of only two intermolecular amide hydrogen bonds at the interface of two monomers. The sensitivity of K_{el} to subtle structural changes and the persistent isodesmic assembly mechanism allow a clear

Received: May 28, 2021

link between monomer structure and assembly thermodynamics as the monomer structure does not undergo significant changes during assembly. This specifically allows us to attribute changes in K_{el} to changes in monomer electronics, making [**n.n**]**pCps** a useful tool for fundamentally understanding what drives self-assembly.

Constrained macrocycles such as [**n.n**]**pCps** are sensitive to small changes in structure that lead to large changes in molecular properties such as strain and conformational flexibility. To provide a self-assembling [**n.n**]**pCp** with stereoelectronic tunability, the central methylene groups of previously synthesized [**3.3**]**pCpTA** were replaced with a sulfur to give 2,11-dithia[3.3]paracyclophane tetracarboxamide (**dt**[**3.3**]**pCpTA**; see Figure 1). It was our hypothesis that

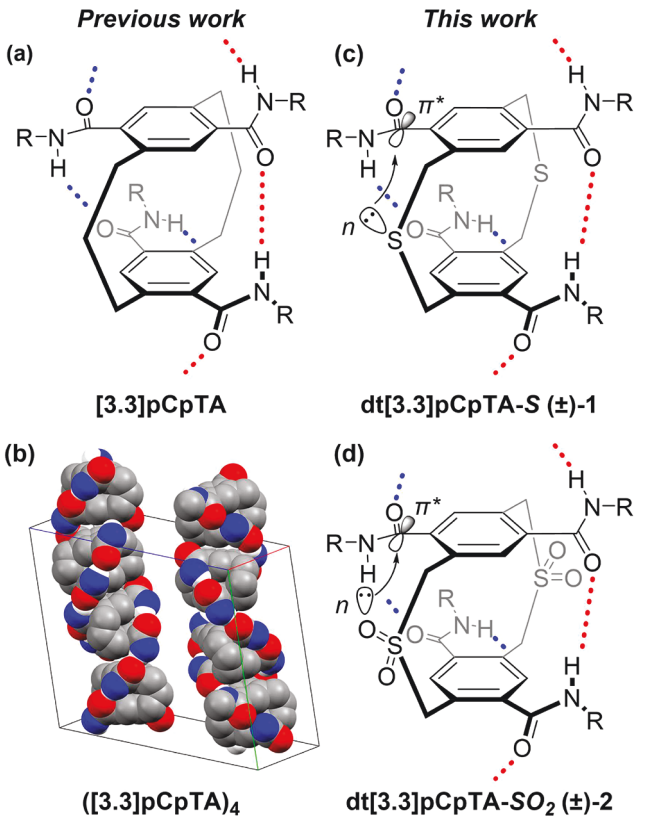

Figure 1. Previously studied self-assembling [**3.3**]**pCpTA** (a) and a representation of its homochiral assemblies (e.g., tetramers) obtained from X-ray crystallography shown as space-filling models with side chains and hydrogen atoms not involved in hydrogen bonding omitted (b, CCDC 1949727). Examples of stereoelectronically tunable **dt**[**3.3**]**pCpTA-***S*(±)-**1** (c) and **dt**[**3.3**]**pCpTA-***SO*$_2$(±)-**2** (d) presented in this work.

conformational, structural, electronic, and stereoelectronic aspects of a self-assembling **dt**[**3.3**]**pCpTA** system could be influenced remotely through the oxidation of the sulfide bridge (**dt**[**3.3**]**pCpTA-***S*, (±)-**1**) to a sulfone bridge (**dt**[**3.3**]-**pCpTA-***SO*$_2$, (±)-**2**).[30,31] An example of the profound influence of sulfur oxidation state on Geländer macrocycle structure and flexibility was recently studied by Mayor and coworkers.[32] In the sulfide bridged **dt**[**3.3**]**pCpTA-***S*(±)-**1**, the bridging sulfur is engaged in a weak $n \rightarrow \pi^*$ interaction with the proximal amide carbonyls. When the sulfide is oxidized to a sulfone (**dt**[**3.3**]**pCpTA-***SO*$_2$(±)-**2**), the sulfone oxygen engages the amide carbonyl in a stronger $n \rightarrow \pi^*$ interaction while not significantly altering the structure of the **dt**[**3.3**]**pCp** skeleton. In a comparison of [**3.3**]**pCpTA** with no $n \rightarrow \pi^*$ interactions to **dt**[**3.3**]**pCpTA-***S* with weak $n \rightarrow \pi^*$ interactions and finally **dt**[**3.3**]**pCpTA-***SO*$_2$ with strong $n \rightarrow \pi^*$ interactions, the trend in K_{el} mirrors the prevalence and strength of the intramolecular contacts. This, as far as we know, is the first example of stereoelectronic effects being used as a secondary feature to tune supramolecular polymer assembly.

RESULTS AND DISCUSSION

Molecular Modeling. Although **dt**[**3.3**]**pCps** are well-known to the chemical literature, a detailed study of their strain energies and conformational dynamics has not been undertaken in the same way as that for [**2.2**]**pCp** and [**3.3**]-**pCps**.[33−37] Alternative studies have been extensively carried out with [3.3]metacyclophanes carrying heteroatoms in the bridge, revealing changes in barriers associated with analogous conformational processes to [**3.3**]**pCps** as a function of linker identity.[38−45] Figure 2 summarizes the structural differences of

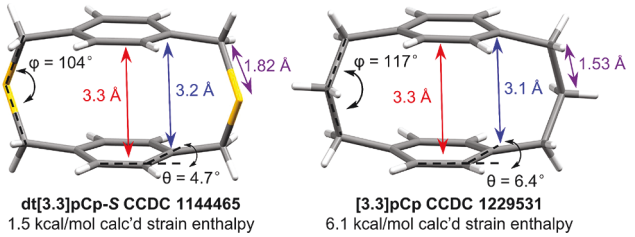

Figure 2. A comparison of the structures from X-ray crystallography, and strain energies (enthalpies) of **dt**[**3.3**]**pCp-***S* (left) and [**3.3**]**pCp** (right).

hydrocarbon [**3.3**]**pCp** and sulfur bridged **dt**[**3.3**]**pCp-***S* obtained by X-ray crystallography. A longer C−S bond compared to C−C bond (1.82 Å vs 1.53 Å) leads to less bent aromatic rings (4.7° compared to 6.4°) in **dt**[**3.3**]**pCp-***S* vs [**3.3**]**pCp**. The result is a decrease in the strain enthalpy of **dt**[**3.3**]**pCp-***S* calculated using homodesmotic reactions (1.5 kcal mol^{-1}, details in SI) compared to the calculated strain enthalpy of 6.1 kcal mol^{-1} for [**3.3**]**pCp**.[33] It is worth noting that the calculated strain enthalpy value for [**3.3**]**pCp** is considerably less than the experimentally determined strain energy of 11.7 kcal mol^{-1} for [**3.3**]**pCp**.[46]

An understanding of the influence of bridge oxidation on **dt**[**3.3**]**pCp** structure and dynamics in the absence of supramolecular assembly was probed initially so that changes in **dt**[**3.3**]**pCpTA** assembly could be more confidently ascribed to electronic effects. Oxidation of the bridge sulfur has been synthetically achieved but fundamentally unexplored and could lead to reduced monomer flexibility, changes in overall **dt**[**3.3**]**pCp** structure, and potential changes in the electronics of the benzene decks. Attempts to synthesize bridge-oxidized **dt**[**3.3**]**pCps** led to incredibly insoluble samples that could not be studied in solution by NMR or other techniques.[47] In fact, only recently has an X-ray structure of a **dt**[**3.3**]**pCp-***SO*$_2$ skeleton been published (with 4 bromine atoms at the 5,8,14,17-positions).[48] In place of suitable experimental studies of insoluble bridge-oxidized **dt**[**3.3**]**pCps**, in-silico studies of the strain energy and conformational flexibility for **dt**[**3.3**]-**pCp-***S* and **dt**[**3.3**]**pCp-***SO*$_2$ were performed to dissect changes in structure and dynamics of **dt**[**3.3**]**pCps** in the absence of

https://doi.org/10.1021/jacs.1c05522
J. Am. Chem. Soc. XXXX, XXX, XXX−XXX

assembly. The ωB97X-D/6-31G level of theory was chosen for DFT calculations, as this functional has been shown to account well for dispersive forces that are crucial for reproducing supramolecular π−π interactions.[49] Homodesmotic reactions designed to determine strain enthalpy of **dt[3.3]pCps** showed that the strain of **dt[3.3]pCps** decreases slightly with bridge oxidation (calc'd strain enthalpy of **dt[3.3]pCp-*SO*$_2$** is 0.8 kcal mol^{-1}).

The main conformational process of **[3.3]pCps**, the *chair/boat* interconversion, has been extensively studied,[34,50,51] while the equivalent process in **dt[3.3]pCps** has only been mentioned as being too fast to measure by ^{1}H NMR at −60 °C.[52] The barrier to **dt[3.3]pCp-*S*** *chair/boat* interconversion (Figure 3) is therefore much lower than that in the

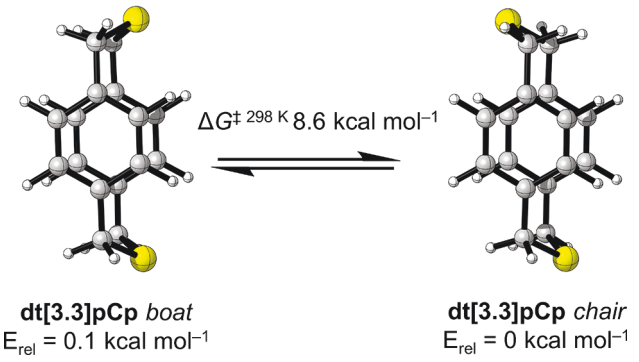

Figure 3. Interconversion between *chair* and *boat* conformers of **dt[3.3]pCps**. DFT calculated relative energies and conformational barrier at the ωB97X-D/6-31G level of theory.

hydrocarbon variant, where interconversion becomes slow on the NMR time scale below −15 °C.[34] Similar substitutions (i.e., S for CH_2) in dithia[3.3]metacyclophanes have increased the conformational flexibility and dynamics compared to their hydrocarbon analogs.[42,43] The increased dynamics in **dt[3.3]-pCp-*S*** are presumably due to the longer C−S bond (Figure 2) and the lack of eclipsing interactions in the *chair/boat* interconversion transition state. If these eclipsing interactions lead to a larger *chair/boat* interconversion barrier, it follows that the barrier in **dt[3.3]pCp-*SO*$_2$** should be larger than that in **dt[3.3]pCp-*S*** as there would be eclipsing interactions with the sulfone oxygen, although they will be smaller than in **[3.3]pCp** due to the longer C−S bond. Calculation of the ground state *chair* and *boat* energies for **dt[3.3]pCp-*S*** and **dt[3.3]pCp-*SO*$_2$**, as well as the *chair/boat* interconversion transition state energies at 298 K, afford $\Delta G^{\ddagger}$ values nearly identical for **dt[3.3]pCp-*S*** (8.6 kcal mol^{-1}) and **dt[3.3]pCp-*SO*$_2$** (8.7 kcal mol^{-1}), indicating there is likely no significant change in conformational freedom upon bridge oxidation (Figures S47−48).

Extensive molecular modeling of **dt[3.3]pCpTAs** revealed the potential for $n \rightarrow \pi^*$ interactions from the lone-pair of the bridge sulfide sulfur or the bridge sulfone oxygen to the π^* orbital of the amide carbonyl. Since pioneering studies by Raines and co-workers,[12,15] this interaction is well understood in the context of proteins and peptides.[9,14,53,54] Donation of electron density from a nonbonding orbital into the π^* orbital of a C=O causes elongation of the C=O bond and an increase in charge localized on the oxygen.[13] The potential for a stronger $n \rightarrow \pi^*$ interaction, at distances shorter than the sum of the van der Waals radii (d) and angles (S/O···C=O, θ) approaching the Bürgi−Dunitz angle (105 ± 5°),[55,56] in **(±)-2** compared to **(±)-1** allows evaluation of the influence of the $n \rightarrow \pi^*$ interaction on amides involved in transannular (intramolecular deck-to-deck) and intermolecular hydrogen bonding. The thermodynamics of supramolecular assembly for **(±)-1** and **(±)-2** could report on the consequences of $n \rightarrow \pi^*$ interactions for hydrogen bond directed assembly in such a constrained system.

Analogous to other **[n.n]pCpTA** systems, the amides in **dt[3.3]pCpTAs** can be arranged in either the *syn-* (*DD*···*AA* array) or *anti-* (*DA*···*AD* array) conformation, depending on whether amides are pointed in the same (*syn-*) or opposite directions (*anti-*). As we have reported previously, the reversibility of **[n.n]pCpTA** assembly and low barriers to amide C_{ar}−C=O rotation that allow fast *syn-/anti-* interconversion results in pathway selection of the *anti*-conformer due to the thermodynamic preference for its assembly despite the energetic similarities between *syn-* and *anti-* monomers.

A model system composed of diastereomeric **dt[3.3]-pCpTA-*SO*** sulfoxides was designed to computationally evaluate differences in $n \rightarrow \pi^*$ interactions from the different bridge substituents (Figure 4). It should be mentioned that

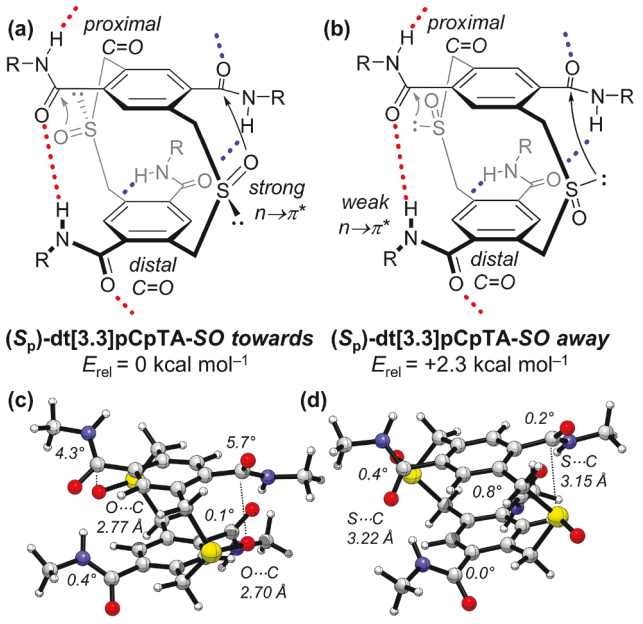

Figure 4. Model system designed to theoretically study differences between $n \rightarrow \pi^*$ interactions with the bridge sulfoxide oxygen pointing *toward* (a) or *away* (b) and the relative energies of each isomer. The DFT optimized geometries (ωB97X-D/6-31G) featuring amide carbonyl puckering angles and S/O···C=O distances in the *toward* (c) and *away* (d) isomers. All calculations were performed in the *chair anti*-conformation.

this molecule was briefly pursued synthetically, but due to the number of possible stereoisomers as well as under- and overoxidation side-products, the prospect of synthesizing and purifying a single pure product quickly proved to be daunting. The model compound **dt[3.3]pCpTA-*SO*** can exist with the bridging sulfoxide pointed *toward* or *away* from the adjacent amides resulting in an $n \rightarrow \pi^*$ interaction from the sulfoxide oxygen in the *toward* isomer or the sulfoxide sulfur in the *away* isomer. By comparing the energies and geometries of the *toward* and *away* isomers of **dt[3.3]pCpTA-*SO*** (Figure 4), the

https://doi.org/10.1021/jacs.1c05522
J. Am. Chem. Soc. XXXX, XXX, XXX−XXX

relative strengths of $n \rightarrow \pi^*$ interactions in (±)-**1** and (±)-**2** will be better understood.

The energy of the *toward* isomer of **dt[3.3]pCpTA**-*SO* is 2.3 kcal mol^{-1} lower than that of the *away* isomer despite the proximity of the sulfoxide and amide groups. This energetic preference is a direct result of the stronger $n \rightarrow \pi^*$ interaction from the bridging sulfoxide oxygen to the nearest amide carbonyl in the *toward* isomer (d = 2.70−2.77 Å, θ = 88−96°) compared to the sulfoxide sulfur in the *away* isomer (d = 3.15−3.22 Å, θ = 84−100°). Further $n \rightarrow \pi^*$ evidence comes from the comparison of amide puckering (deviation of the carbonyl atom from the C_{ar}−N−O plane, Θ) for amides in the same molecule. In the *toward* isomer, the proximal carbonyl receives nonbonding electron donation from the sulfoxide oxygen and puckers toward the sulfoxide by 4.3−5.7°. The other amides which do not receive electron donation maintain their planarity with Θ ∼ 0°. The amides in the *away* isomer which only receive donation from the sulfoxide sulfur also maintain relative planarity with Θ up to 0.8°. These results indicate that the strength of the $n \rightarrow \pi^*$ interaction in the sulfone (±)-**2** should be considerably stronger than that in the sulfide (±)-**1**. Similar computational analyses of (S_p)-**1** and (S_p)-**2** reveal the presence of stronger $n \rightarrow \pi^*$ interactions in (S_p)-**2**. NBO analysis was performed to confirm orbital overlap between the nonbonding orbitals of the sulfide or sulfone and the amide π^* (Figure 5), showing that the sulfone in (S_p)-**2** results in better orbital overlap when compared to (S_p)-**1**.

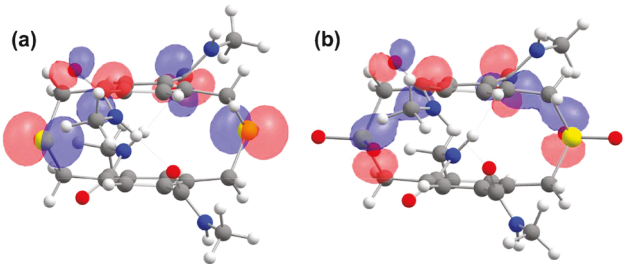

Figure 5. Orbital plots of the sulfur nonbonding orbitals and the amide π^* orbitals in (S_p)-**1** (a) and the sulfone oxygen nonbonding orbitals and the amide π^* orbitals in (S_p)-**2** (b) obtained from NBO analysis.

Energies of **dt[3.3]pCpTAs** obtained from DFT calculations reveal a thermodynamic preference for the *chair* conformers of both **1** and **2**, with the *chair anti*-conformer of **1** favored by 0.2 kcal mol^{-1} and the *chair syn*-conformer of **2** favored by 0.6 kcal mol^{-1} in the gas phase. Optimization of dimers of **1** and **2** reveals a slightly larger interaction energy for the **2** *anti*-dimer (−45.9 kcal mol^{-1}) compared to the **1** *anti*-dimer (−44.4 kcal mol^{-1}) indicating potential for stronger supramolecular assembly of **2**. Energies of the *syn*-dimers for both **1** and **2** were >5 kcal mol^{-1} higher in energy than the *anti*-conformers, indicating the thermodynamic preference for *anti*-assembly, consistent with previously studied **[n.n]pCpTAs** (Figure 6).[24−26]

Synthesis. The synthetic chemistry of **dt[3.3]pCps** differs from that of hydrocarbon variants, as **dt[3.3]pCps** are readily prepared by macrocyclic coupling of extensively prefunctionalized 1,4-bis(bromomethyl)benzenes and 1,4-bis(thiomethyl)benzenes.[57−64] Oftentimes, the **dt[3.3]pCps** then undergo sulfur extrusion to give the hydrocarbon bridged **[2.2]pCps** with precise regiochemical control.[65−71]

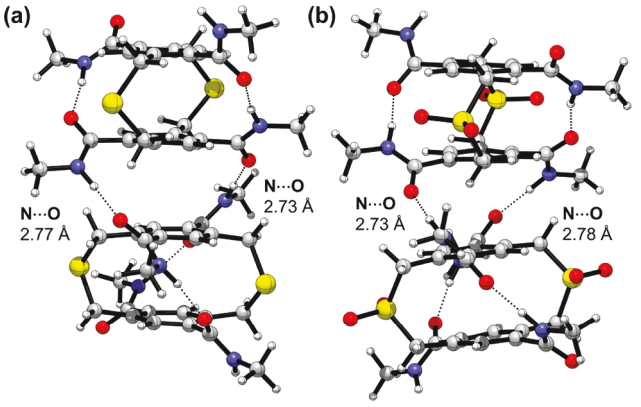

Figure 6. DFT optimized geometries of (S_p)-**1** (a) and (S_p)-**2** (b) dimers with intermolecular hydrogen bond (N···O) distances highlighted.

Retrosynthetic analysis of (±)-**1** and (±)-**2** led to the advanced tetra-carboxylic acid intermediate (±)-**3a** which could come from hydrolysis of the tetra-ester (±)-**4a**. Although **dt[3.3]pCps** with ester substituents are known in the literature,[63,72−74] an example with decks comprising two ester units each (for a total of four) was unknown. Synthesis of (±)-**4a** necessitated the development of new macrocyclization chemistry and could be envisioned to come from the known thiol **5a** and its precursor bromide **6**, published in previous work by Staab and co-workers.[63] The synthesis of target **dt[3.3]pCpTAs** beginning from **6** is depicted in Scheme 1.

Synthesis of **5a** beginning from building block **6**,[75] available in 4 steps from commercial 2,5-dibromo-*p*-xylene, proceeded in the literature through a diazomethane esterification of the corresponding 1,4-bis(thiomethyl)terephthalic acid.[63] As a safer alternative, we utilized $TMSCHN_2$ for the synthesis of **5a**, but to our dismay, the reaction proceeded in poor yields. Attempts at Fischer esterification in methanol and sulfuric acid at reflux led to the presumably stable, but unknown to the literature, bis(thiolactone) which could only be characterized by ^{1}H NMR, FT-IR, and GC-MS due to its incredibly poor solubility (see SI). Despite the poor conversion of **6** to **5a**, enough **5a** was accessed to attempt synthesis of (±)-**4a** by 1:1 coupling of **5a** and **6**. This reaction proceeded well to give a mixture of the desired 5,8,14,17-regioisomer (±)-**4a** and its achiral *gem*- 5,8,15,18-regioisomer **4b** in a ca. 5:1 ratio in favor of (±)-**4a**. Chemical intuition dictates that (±)-**4a** should be the most stable regioisomer due to the minimization of transannular steric interactions that are present in **4b.** The regiochemistry of (±)-**4a** and **4b** could be further confirmed experimentally by comparison of chemical shifts and coupling constants with previously known tetrabromo-**dt[3.3]pCps** whose structures were confirmed by X-ray crystallography (Figure S1 and S2).[76]

Although compound (±)-**4a** was obtained in small quantities, a route to (±)-**4a** on larger scale was desired for synthesis of (±)-**1** and (±)-**2**. Revision of the synthetic route took advantage of the *in situ* deprotection of a thioacetate group of **5b** to unveil a masked thiolate followed by substitution and macrocyclization with one equivalent of **6** to give a mixture of (±)-**4a** and **4b**. The desired regioisomer (±)-**4a** could be separated by careful fractional crystallization from DCM/MeOH but was generally carried forward as a mixture and separated as the final target (±)-**1** through column chromatography and fractional crystallization. Hydrol-

https://doi.org/10.1021/jacs.1c05522
J. Am. Chem. Soc. XXXX, XXX, XXX−XXX

Scheme 1. Synthesis of dt[3.3]pCpTA-*S* (±)-1 and dt[3.3]pCpTA-*SO*$_2$ (±)-2[a]

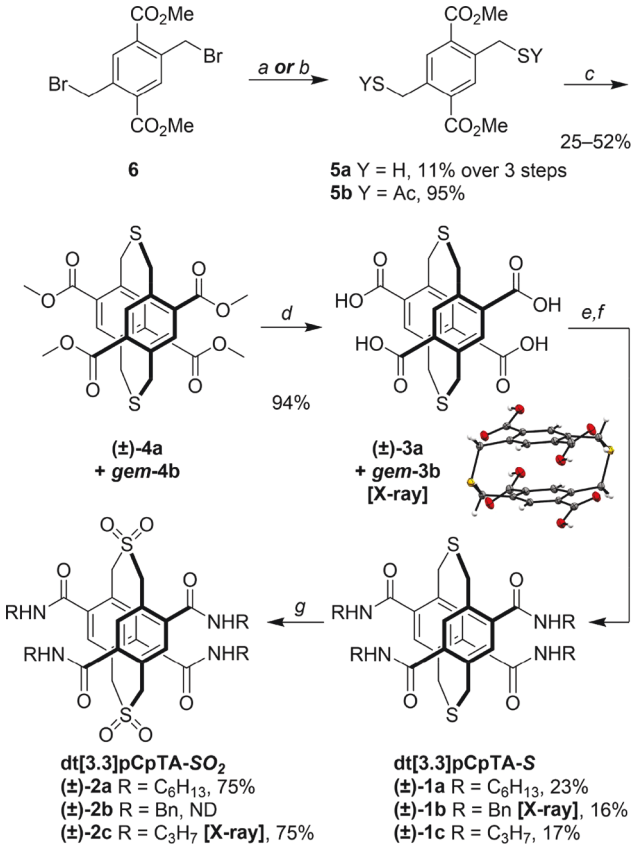

[a]Reagents: *a* thiourea, EtOH, reflux then aq. $NaHCO_3$, reflux, then $TMSCHN_2$, THF, rt; *b* potassium thioacetate, THF, rt; *c* **6** and **5a** or **5b** (1:1 in DCM) slow addition to KOH (2.2 equiv) in 1 L MeOH; *d* KOH, THF, EtOH, H_2O (1:1:1); *e* $(COCl)_2$, DMF (cat.), THF, rt; *f* RNH_2 (excess), NEt_3 (excess), THF, rt; *g* *m*-CPBA (10 equiv), $CHCl_3$, rt.

ysis of (±)-**4a** and mixtures of (±)-**4a** and **4b** to (±)-**3a** and mixtures of (±)-**3a** and **3b** proceeded equally well. Attempts to crystallize tetra-carboxylic acid (±)-**3a** from a crude mixture of (±)-**3a** and **3b** by vapor diffusion of water into a DMSO solution led to crystallization of the minor component **3b** whose structure was confirmed by single crystal X-ray diffraction (see Supporting Info). Comparison of the ^{1}H NMR spectra of (±)-**3a**, **3b**, and their mixture confirmed the structure of (±)-**3a** and therefore the structure of (±)-**4a**. Synthesis of (±)-**1** was completed by amide bond formation through an acyl chloride intermediate formed from (±)-**3a** and condensation with the appropriate primary amine. Oxidation of (±)-**1** to (±)-**2** could be readily accomplished with excess *m*-CPBA.

Compound (±)-**1a** with R = *n*-hexyl gave good solubility in moderately polar $CHCl_3$ and nonpolar methylcyclohexane (MCH). Compound (±)-**2a** also exhibited good solubility in $CHCl_3$, but bridge oxidation significantly reduced its solubility in MCH or $CHCl_3$/MCH mixtures. Aromatic side chains in (±)-**1b** and (±)-**2b** (R = benzyl) were introduced to allow single crystal growth for X-ray diffraction. Unfortunately, compound (±)-**2b** exhibited very poor solubility in nearly all common organic solvents and attempts at single crystal growth were not successful. To circumvent the poor crystallinity of (±)-**2b**, the benzyl side chain was exchanged for a *n*-propyl side chain in compound (±)-**2c** to allow for single crystal growth.

X-ray Crystallography. Single-crystal X-ray diffraction is crucial for evaluating structural changes expected to report on the presence and strength of $n \rightarrow \pi^*$ interactions in self-assembling **dt[3.3]pCpTAs**.[77] Single crystals of (±)-**1b** were grown by slow evaporation from an ethanol/ethyl acetate solution. The unit cell of (±)-**1b** is composed of 8 molecules of **1b** (4 R_p, and 4 S_p) in the *anti*-amide conformation. Significant disorder is present in the sulfur bridge in both molecules of the asymmetric unit (S_{2a}/$S_{2a'}$ 53%/47% and S_{4a}/$S_{4a'}$ 60%/40%) representing a ca. 1:1 combination of *chair* and *boat* conformers.

Analysis of monomeric (R_p)-**1b** from X-ray crystallography is depicted in Figure 7a. All amides are participating in

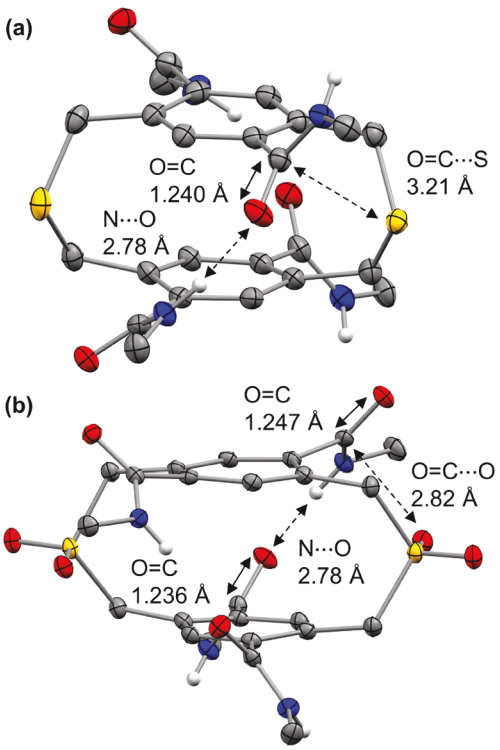

Figure 7. ORTEP of (R_p)-**1b** in the *boat anti*-conformation (a) and ORTEP of (S_p)-**2c** in the *chair syn*-conformation (b) from X-ray crystallography. Average distances (except for C=O distance in **2c**) shown highlight similar transannular H-bonding distances and changes in $n \rightarrow \pi^*$ interactions in each. Ellipsoids shown at 50% probability, side chains and hydrogens not involved in hydrogen bonding omitted for clarity. Atom color code C gray, H white, O red, N blue, S yellow.

transannular and intermolecular self-complementary hydrogen bonding (i.e., N–H···O=C, N···O distance 2.75–2.81 Å). The bridge sulfur in **1b** is engaged in a weak $n \rightarrow \pi^*$ interaction with the closest amide carbonyl (S···C=O distance of 3.16–3.25 Å, S···C=O angle 82–102°). The S···C=O angles are expected to occupy a range of values in a dynamic solution environment that varies with the C_{ar}–C=O rotation, while the S···C=O distances are expected to be restricted as any further displacement could introduce strain to the cyclophane scaffold. The amide C=O pucker (measured as deviation from the C_{ar}–N–O plane toward the nonbonding donor) ranges from 0° in

https://doi.org/10.1021/jacs.1c05522
J. Am. Chem. Soc. XXXX, XXX, XXX–XXX

amides distal to the sulfide to 3° in amides proximal to the sulfide, although the bridge disorder means that all amides are likely receiving a nonequivalent portion of electron donation from the bridge sulfur atoms. The C=O bond length ranges from 1.236−1.242 Å and does not seem to be correlated to the S···C=O interaction as the shortest and longest C=O bonds are both proximal to the bridge sulfur.

Unlike the crystal packing in all previous self-assembling [**n.n**]**pCps**, which featured only homochiral assemblies, heterochiral interactions are present in the crystal structure of (±)-**1b**. Hydrogen bonding occurs between alternating pairs of homochiral dimers (i.e., $[(R_p)$-**1b**$]_2\cdots[(S_p)$-**1b**$]_2\cdots[(R_p)$-**1b**$]_2$) to propagate 1-D stacks, with different $\pi\cdots\pi$ distances (centroid···centroid) for homochiral (4.05 Å) and heterochiral (4.33 Å) dimers. The enthalpic penalty of the heterochiral dimerization in the crystal structure of (±)-**1b** is compensated for by other intermolecular interactions (Figure 8a) leading to

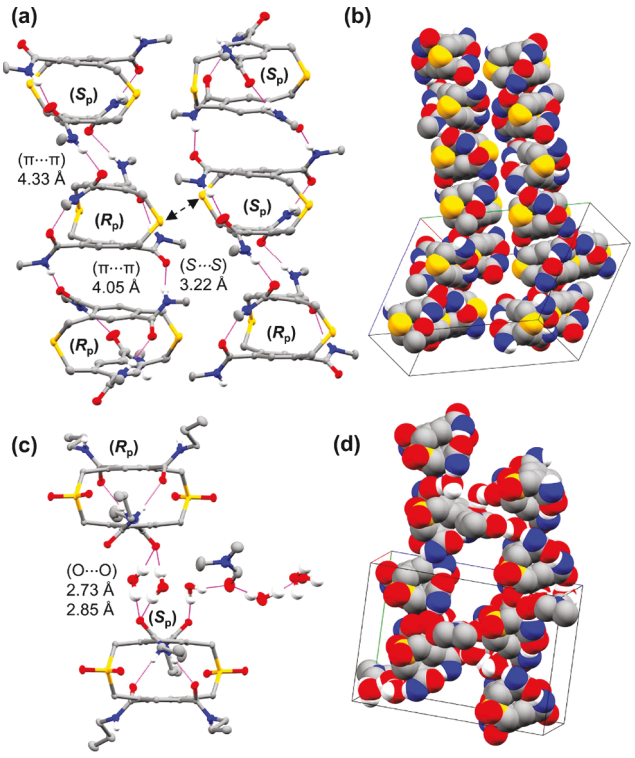

Figure 8. Hydrogen bond propagation in the crystal structure of (±)-**1b**, with $\pi\cdots\pi$ (centroid···centroid) and intercolumnar S···S distances reported (a). Crystal packing of (±)-**1b** shown as space-filling model (b). Hydrogen bond propagation in the crystal structure of (±)-**2c** through water and DMF molecules (c). Crystal packing of (±)-**2c** shown as space-filling model (d). Side chains and hydrogen atoms not involved in hydrogen bonding omitted for clarity.

the observed unit cell and assembly structure (Figure 8b). These include a cancellation of monomer dipoles between the two enantiomers involved in the heterochiral interaction and an intercolumnar S···S interaction between two monomers with opposing dipoles. Preliminary DFT calculations of the *anti*-conformer of **1** show a pronounced molecular orbital localization on the bridging sulfur atom with which the C=O dipoles are aligned (Figure S55). The polarizability of this bridge sulfur atom in **1** appears unfavorable due to the formation of heterochiral dimers with lower interaction energies which are mitigated by dipole cancellation and S···S interactions in the crystal packing of (±)-**1b**. DFT calculations of the heterochiral dimer observed in **1b** reveal a significant 3.5 kcal mol^{-1} mismatch penalty (see Table S14). This mismatch penalty is large enough to engender homochirality to the dynamic solution-phase assembly of **1a**.[78] Worth noting is the increase in mismatch penalty to 7.5 kcal mol^{-1} calculated for a heterochiral dimer of **2**, showing that bridge oxidation can change energetic preferences for homochiral vs heterochiral assembly by altering the polarizability of the bridge sulfur.

Single crystals of (±)-**2c** were grown by cooling a DMF/H_2O solution of (±)-**2c** over the course of several weeks at −10 °C. The asymmetric unit of the crystal of (±)-**2c** is composed of one enantiomeric molecule of **2c** along with one molecule of DMF and four molecules of H_2O. As a result of the polar solvent used for crystal growth, the crystal packing of (±)-**2c** is largely dominated by intermolecular hydrogen bonding to DMF and H_2O solvent molecules, with H_2O forming H-bonded bridges between molecules of **2c**. Despite the presence of several hydrogen bond capable solvent molecules, transannular amide hydrogen bonding is maintained (N···O distance 2.75−2.81 Å). Interestingly, oxidation of the bridge sulfur to a sulfone results in a lack of bridge disorder as (±)-**2c** in the crystal exists solely in the *chair* conformation. Another surprising feature of the X-ray structure of (±)-**2c** is the presence of the *syn*-amide conformation: the first experimental observation in thus-synthesized self-assembling [**n.n**]**pCps**. It is likely that the *syn*-conformation of (±)-**2c** is enabled by its solvation by highly polar solvents during crystal growth and that *syn-/anti-* interconversion still occurs in solution. Analysis of monomeric (R_p)-**2c** from X-ray crystallography is depicted in Figure 7b.

Evidence for the stronger $n \rightarrow \pi^*$ interaction expected in (±)-**2c** includes the fact that the S=O···C distance of the sulfone oxygen to the amide carbonyl (2.78−2.86 Å) is considerably shorter than the S···C distances in (±)-**1b**. The O···C=O angle (93−95°) is also reasonably close to the range expected for an $n \rightarrow \pi^*$ interaction. It is worth restating that the S=O···C distances are not expected to vary due to the rigidity of the cyclophane, whereas the O···C=O angles would be dependent on the C_{ar}−C=O rotation which is expected to be dynamic. The C=O pucker in (±)-**2c** is also present, with deviations from the C_{ar}−N−O plane varying from 1.8−2.5° for amides proximal to the sulfone and 1.2° for amides distal to the sulfone. Perhaps the most convincing crystallographic evidence of a stronger $n \rightarrow \pi^*$ interaction in (±)-**2c** is the elongation of the amide C=O bond. In the amides engaged in $n \rightarrow \pi^*$ interactions with the sulfone oxygen, the C=O bond is 0.011 Å longer than in those which are not engaged in $n \rightarrow \pi^*$ interactions (1.236 vs 1.247 Å). It has been noted that amide C=O's which accept $n \rightarrow \pi^*$ interactions have an increase in partial negative charge on the oxygen atom, making them better H-bond acceptors. This can rationalize the preference for the proximal amide (better H-bond acceptor) to engage in intermolecular H-bonding to H_2O solvent molecules instead of transannular H-bonding across a restricted distance in **2c**. The result is an amide C=O which experiences bifurcated H-bonding to two separate H_2O molecules that form a water bridge to another molecule of opposite configuration (i.e., (R_p)-**1c**···2H_2O···(S_p)-**1c**, O···O distance 2.73−2.85 Å, see Figure 8c). Intermolecular hydrogen bonding to solvent molecules leads to a vastly different unit cell and assembly structure for (±)-**2c** in the crystal (Figure 8d), with no appreciable $\pi\cdots\pi$ interactions.

https://doi.org/10.1021/jacs.1c05522
J. Am. Chem. Soc. XXXX, XXX, XXX−XXX

Solution Studies. Supramolecular assembly of (±)-**1a** and (±)-**2a** was evaluated using solution studies in moderately polar $CHCl_3$ and nonpolar (methyl)cyclohexane. Solutions of (±)-**1a** and (±)-**2a** in $CDCl_3$ exhibit simplified ^{1}H NMR spectra as amide rotation and bridge conformational interconversion are fast on the NMR time scale. The oxidation state of the sulfur bridge profoundly influences the ^{1}H NMR chemical shifts of compounds (±)-**1a** and (±)-**2a** (Figure 9).

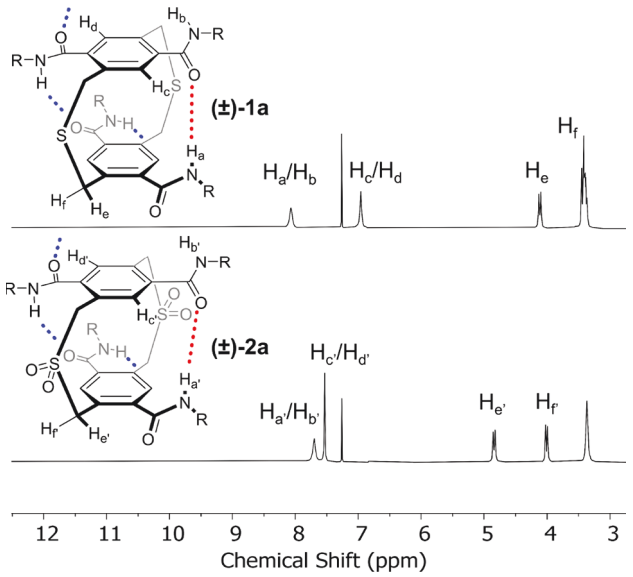

Figure 9. Changes in the ^{1}H NMR spectra (12 mM in $CDCl_3$) of **dt[3.3]pCpTAs** upon bridge oxidation of sulfide (±)-**1a** (top) to sulfone (±)-**2a** (bottom).

The benzylic bridge resonances α to the sulfur (H_e and H_f in (±)-**1a** and $H_{e'}$ and $H_{f'}$ in (±)-**2a**) are expectedly shielded in (±)-**1a** compared to (±)-**2a** at comparable concentrations. The aromatic C−H resonance (H_c/H_d in (±)-**1a** and $H_{c'}/H_{d'}$ in (±)-**2a**) becomes significantly deshielded upon bridge oxidation moving from δ 6.96 ppm in (±)-**1a** to δ 7.54 ppm in (±)-**2a** at 12 mM in $CDCl_3$. Interestingly, the opposite trend of chemical shift change upon oxidation is observed for the N−H resonance (H_a/H_b in (±)-**1a** and $H_{a'}/H_{b'}$ in (±)-**2a**) that becomes shielded from δ 8.07 ppm in (±)-**1a** to δ 7.70 ppm in (±)-**2a** under the same conditions. This unusual change in chemical shift for $H_{a'}/H_{b'}$ in (±)-**2a** is a direct result of the proximity of the S=O atom and the amide C=O engaged in an $n \rightarrow \pi^*$ interaction. The chemical shift of the amide N−H for **dt[3.3]pCpTAs** in $CDCl_3$ represents a time-average of transannular, intermolecular, and solvent-exposed environments. Increasing concentration shifts the equilibrium toward assembly and allows the determination of association constants. Assignment of individual resonances from (±)-**1a** in the assembled state can be found in Figure 10a. Variable concentration ^{1}H NMR of (±)-**1a** shows a change in the amide N−H chemical shift (H_a/H_b) from 7.34 ppm at 0.025 mM to 8.31 ppm at 24 mM indicating an increase in intermolecular hydrogen bonding at higher concentrations (Figure 10b). A shift in the aromatic C−H resonance (H_c/H_d) from 7.22 ppm at 0.025 mM to 6.85 ppm at 24 mM indicates an increase in π-stacking such as that observed in the X-ray structure of (±)-**1b**. Consistent with what is observed in other self-assembling **[n.n]pCpTA** systems, the data adheres to an isodesmic mechanism, and offers an elongation constant K_{el} of

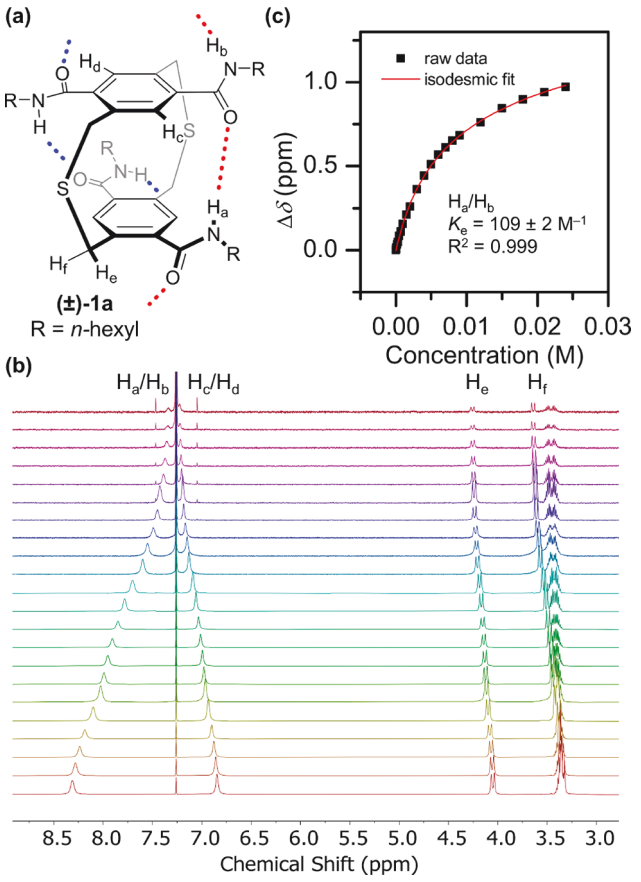

Figure 10. Chemical shift assignments for (±)-**1a** in the assembled state (a) and the variable concentration ^{1}H NMR of (±)-**1a** from 0.025−24 mM in $CDCl_3$ (b). Isodesmic fit of the change in the amide N−H chemical shift H_a/H_b to give K_e (c).

109 ± 2 M^{-1} (Figure 10c).[22,25] The value of K_{el} for (±)-**1b** is ∼6-fold higher than that for the analogous **[3.3]pCpTA** under identical conditions.[25]

An analogous experiment with (±)-**2a** (peak assignments in Figure 11a) shows similar trends including deshielding of the amide N−H ($H_{a'}/H_{b'}$) from 6.91 ppm at 0.025 mM to 7.85 ppm at 24 mM and shielding of the aromatic C−H ($H_{c'}/H_{d'}$) from 7.72 ppm at 0.025 mM to 7.51 ppm at 24 mM (Figure 11b). Fitting the concentration-dependent change in N−H chemical shift of (±)-**2a** to an isodesmic model reveals a larger association constant of 224 ± 8 M^{-1} (Figure 11c).

Despite the presence of the *syn*-conformer in the crystal structure of (±)-**2a**, assembly of both (±)-**1a** and (±)-**2a** is expected to proceed through pathway selection and isodesmic assembly of the lowest energy *anti*-conformer in solution, likely resulting in homochiral assemblies due to the large calculated mismatch penalties.

Electronic transitions that are expected to be altered with bridge oxidation from (±)-**1a** to (±)-**2a** were examined with UV−vis spectroscopy. Although the insolubility of (±)-**2a** in MCH only allowed study in $CHCl_3$ where the solvent absorbs in the same range of the target molecule, time-dependent DFT calculations reveal an expected change in the absorbance with bridge oxidation (Figure S22).

The relevant stretching frequencies of the amide bond (i.e., C=O and N−H) can inform on both their supramolecular and stereoelectronic environment (Figure 12). Supramolecular assembly is confirmed by concentration-dependent changes

https://doi.org/10.1021/jacs.1c05522
J. Am. Chem. Soc. XXXX, XXX, XXX−XXX

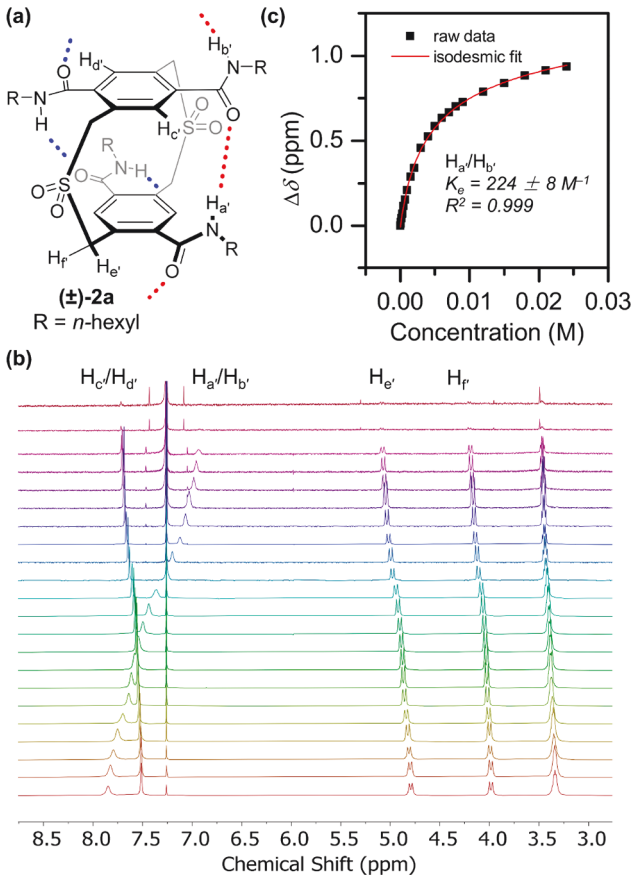

Figure 11. Chemical shift assignments for (±)-**2a** in the assembled state (a) and the variable concentration ^{1}H NMR of (±)-**2a** from 0.025−24 mM in $CDCl_3$ (b). Isodesmic fit of the change in the amide N−H chemical shift $H_{a'}/H_{b'}$ to give K_e (c).

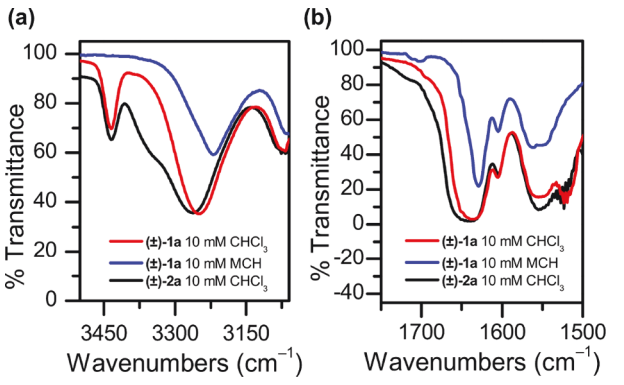

Figure 12. Infrared spectra of the N−H region (a) and the C=O region (b) of (±)-**1a** and (±)-**2a** 10 mM in $CHCl_3$ and methylcyclohexane (MCH).

in the infrared spectra of (±)-**1a** and (±)-**2a** consistent with what was observed by ^{1}H NMR. In solutions of $CHCl_3$, (±)-**1a** exhibits two N−H stretching frequencies corresponding to a solvent exposed N−H (~3434 cm^{-1}) and broad hydrogen bonded N−H which shifts to lower energy upon an increase in concentration due to an increase in intermolecular hydrogen bonding (3263 cm^{-1} at 1 mM, 3243 cm^{-1} at 30 mM). Nonpolar solvents such as methylcyclohexane (MCH) favor polymeric assemblies of (±)-**1a** as confirmed by FT-IR, where (±)-**1a** exhibits only a concentration-*independent* hydrogen bonded N−H at 3219 cm^{-1}: the same frequency as the N−H in solid (±)-**1a** where all N−H's are engaged in hydrogen bonding. Infrared spectra of (±)-**2a** reveal changes in the amide environment that result from a strong $n \rightarrow \pi^*$ interaction.

The N−H region of (±)-**2a** in $CHCl_3$ features the same solvated N−H (3434 cm^{-1}) and broad concentration-dependent hydrogen bonded N−H. At similar concentrations, the hydrogen bonded N−H of (±)-**2a** occurs at higher energy (3273 cm^{-1} at 1 mM). Increasing concentrations of (±)-**2a** result in the hydrogen bonded N−H shifting to lower energies (3258 cm^{-1} at 30 mM) accompanied by the appearance of a high energy shoulder at ~3340 cm^{-1}, becoming prominent at higher concentrations (see Figure S15). In solid (±)-**2a**, the shoulder is present, meaning it still corresponds to a hydrogen bonded N−H. Upon closer inspection of the calculated frequencies of optimized dimers of **1** and **2**, the shoulder is a direct result of the $n \rightarrow \pi^*$ interaction. Amides engaged in $n \rightarrow \pi^*$ interactions exhibit N−H stretches at higher frequencies than those that are not engaged in $n \rightarrow \pi^*$ interactions (see Table S4). The infrared spectrum of (±)-**2a** is direct evidence for the influence of $n \rightarrow \pi^*$ interactions on supramolecular assembly, with distinct N−H stretches for amides engaged in $n \rightarrow \pi^*$ interactions (high energy shoulder) and for amides not engaged in $n \rightarrow \pi^*$ interactions (low energy absorption).

Stretching frequencies of the amide C=O are expected to be weakened in the presence of $n \rightarrow \pi^*$ interactions, but the C=O stretches in (±)-**1a** and (±)-**2a** occur at roughly the same energy (1630−1640 cm^{-1}), presumably due to transannular and intermolecular hydrogen bonding present in both.

CONCLUSIONS

A new set of self-assembling **dt[3.3]pCpTAs** differing in their bridge oxidation state has been designed, synthesized, and characterized. The isodesmic supramolecular polymerization of **dt[3.3]pCpTAs** is altered by the presence and strength of a stereoelectronic interaction between the bridging atom and the amide hydrogen bonding units. The attractive $n \rightarrow \pi^*$ interaction can help to stabilize the assembling conformers of (±)-**1** and (±)-**2** and polarize the amide C=O to make it a better H-bond acceptor. The result is an increase in the elongation constant for **dt[3.3]pCpTAs** compared to that for their carbocyclophane analog **[3.3]pCpTA**. A further increase in elongation constant is observed for the sulfone (±)-**2** with the stronger $n \rightarrow \pi^*$ interaction compared to that for sulfide (±)-**1** with the weaker $n \rightarrow \pi^*$ interaction. The impact of the $n \rightarrow \pi^*$ interaction on amide H-bond donors such as the N−H's in (±)-**2** was observed in the infrared spectra and computationally, and although the origin of the changes in N−H stretching frequency is unclear, study of model compounds is currently underway. The design principle of tuning supramolecular assembly through stereoelectronic effects in **[n.n]pCp** systems is expected to be amenable to different bridging atoms and hydrogen bonding units, and we look forward to reporting further examples in due course.

ASSOCIATED CONTENT

Supporting Information

The Supporting Information is available free of charge at https://pubs.acs.org/doi/10.1021/jacs.1c05522.

https://doi.org/10.1021/jacs.1c05522
J. Am. Chem. Soc. XXXX, XXX, XXX−XXX

Experimental and computational details, synthetic procedures, copies of NMR spectra, association constant determination, IR, and UV−vis spectra (PDF)

Accession Codes

CCDC 2086347−2086349 contain the supplementary crystallographic data for this paper. These data can be obtained free of charge via www.ccdc.cam.ac.uk/data_request/cif, or by emailing data_request@ccdc.cam.ac.uk, or by contacting The Cambridge Crystallographic Data Centre, 12 Union Road, Cambridge CB2 1EZ, UK; fax: +44 1223 336033.

AUTHOR INFORMATION

Corresponding Author

Ronald K. Castellano − *George & Josephine Butler Polymer Research Laboratory, Center for Macromolecular Science & Engineering, Department of Chemistry, University of Florida, Gainesville, Florida 32611-7200, United States;* orcid.org/0000-0003-4322-9932; Email: castellano@chem.ufl.edu

Authors

Will R. Henderson − *George & Josephine Butler Polymer Research Laboratory, Center for Macromolecular Science & Engineering, Department of Chemistry, University of Florida, Gainesville, Florida 32611-7200, United States;* orcid.org/0000-0003-4791-3184

Guancen Liu − *George & Josephine Butler Polymer Research Laboratory, Center for Macromolecular Science & Engineering, Department of Chemistry, University of Florida, Gainesville, Florida 32611-7200, United States*

Khalil A. Abboud − *George & Josephine Butler Polymer Research Laboratory, Center for Macromolecular Science & Engineering, Department of Chemistry, University of Florida, Gainesville, Florida 32611-7200, United States*

Complete contact information is available at: https://pubs.acs.org/10.1021/jacs.1c05522

Notes

The authors declare no competing financial interest.

ACKNOWLEDGMENTS

This work is dedicated to the memory of Prof. François Diederich. Acknowledgement is made to the National Science Foundation (NSF, CHE-1904534) for supporting this research. K.A.A. wishes to acknowledge the NSF and the University of Florida for funding of the X-ray diffractometer through grant CHE-1828064. We acknowledge University of Florida (UF) Research Computing for providing computational resources and support that have contributed to the research results reported in this publication (https://www.rc.ufl.edu). The mass spectrometric data were obtained by the UF Department of Chemistry Mass Spectrometry Research and Education Center supported, in part, by the National Institutes of Health (NIH S10 OD021758-01A1). We would also like to thank Dr. Ion Ghiviriga and the UF Center for Nuclear Magnetic Resonance Spectroscopy for providing equipment and support that have contributed to these published results.

REFERENCES

(1) Brunsveld, L.; Folmer, B. J.; Meijer, E. W.; Sijbesma, R. P. Supramolecular polymers. *Chem. Rev.* **2001**, *101* (12), 4071−4098.

(2) Wang, F.; Han, C.; He, C.; Zhou, Q.; Zhang, J.; Wang, C.; Li, N.; Huang, F. Self-Sorting Organization of Two Heteroditopic Monomers to Supramolecular Alternating Copolymers. *J. Am. Chem. Soc.* **2008**, *130* (34), 11254−11255.

(3) Greciano, E. E.; Matarranz, B.; Sanchez, L. Pathway Complexity Versus Hierarchical Self-Assembly in N-Annulated Perylenes: Structural Effects in Seeded Supramolecular Polymerization. *Angew. Chem., Int. Ed.* **2018**, *57* (17), 4697−4701.

(4) Kar, H.; Gehrig, D. W.; Allampally, N. K.; Fernández, G.; Laquai, F.; Ghosh, S. Cooperative supramolecular polymerization of an amine-substituted naphthalene-diimide and its impact on excited state photophysical properties. *Chem. Sci.* **2016**, *7* (2), 1115−1120.

(5) Wehner, M.; Röhr, M. I. S.; Bühler, M.; Stepanenko, V.; Wagner, W.; Würthner, F. Supramolecular Polymorphism in One-Dimensional Self-Assembly by Kinetic Pathway Control. *J. Am. Chem. Soc.* **2019**, *141* (14), 6092−6107.

(6) Sarkar, A.; Behera, T.; Sasmal, R.; Capelli, R.; Empereur-Mot, C.; Mahato, J.; Agasti, S. S.; Pavan, G. M.; Chowdhury, A.; George, S. J. Cooperative Supramolecular Block Copolymerization for the Synthesis of Functional Axial Organic Heterostructures. *J. Am. Chem. Soc.* **2020**, *142* (26), 11528−11539.

(7) Yano, K.; Itoh, Y.; Araoka, F.; Watanabe, G.; Hikima, T.; Aida, T. Nematic-to-columnar mesophase transition by in situ supramolecular polymerization. *Science* **2019**, *363* (6423), 161−165.

(8) Spitzer, D.; Rodrigues, L. L.; Straßburger, D.; Mezger, M.; Besenius, P. Tuneable Transient Thermogels Mediated by a pH- and Redox-Regulated Supramolecular Polymerization. *Angew. Chem., Int. Ed.* **2017**, *56* (48), 15461−15465.

(9) Newberry, R. W.; Raines, R. T. The n→π^* Interaction. *Acc. Chem. Res.* **2017**, *50* (8), 1838−1846.

(10) Glendening, E. D.; Landis, C. R.; Weinhold, F. Natural bond orbital methods. *Wiley Interdiscip. Rev.: Comput. Mol. Sci.* **2012**, *2* (1), 1−42.

(11) Alabugin, I. V. *Stereoelectronic Effects: A Bridge Between Structure and Reactivity*. John Wiley & Sons: 2016.

(12) Bretscher, L. E.; Jenkins, C. L.; Taylor, K. M.; DeRider, M. L.; Raines, R. T. Conformational Stability of Collagen Relies on a Stereoelectronic Effect. *J. Am. Chem. Soc.* **2001**, *123* (4), 777−778.

(13) DeRider, M. L.; Wilkens, S. J.; Waddell, M. J.; Bretscher, L. E.; Weinhold, F.; Raines, R. T.; Markley, J. L. Collagen Stability: Insights from NMR Spectroscopic and Hybrid Density Functional Computational Investigations of the Effect of Electronegative Substituents on Prolyl Ring Conformations. *J. Am. Chem. Soc.* **2002**, *124* (11), 2497−2505.

(14) Bartlett, G. J.; Choudhary, A.; Raines, R. T.; Woolfson, D. N. n→π^* interactions in proteins. *Nat. Chem. Biol.* **2010**, *6* (8), 615−620.

(15) Holmgren, S. K.; Taylor, K. M.; Bretscher, L. E.; Raines, R. T. Code for collagen's stability deciphered. *Nature* **1998**, *392* (6677), 666−667.

(16) Kilgore, H. R.; Olsson, C. R.; D'Angelo, K. A.; Movassaghi, M.; Raines, R. T. n→π^* Interactions Modulate the Disulfide Reduction Potential of Epidithiodiketopiperazines. *J. Am. Chem. Soc.* **2020**, *142* (35), 15107−15115.

(17) Lampkins, A. J.; Abdul-Rahim, O.; Li, H.; Castellano, R. K. Enhanced Small-Molecule Assembly through Directional Intramolecular Forces. *Org. Lett.* **2005**, *7* (20), 4471−4474.

(18) Li, H.; Homan, E. A.; Lampkins, A. J.; Ghiviriga, I.; Castellano, R. K. Synthesis and Self-Assembly of Functionalized Donor-σ-Acceptor Molecules. *Org. Lett.* **2005**, *7* (3), 443−446.

(19) Sumpter, B. G.; Meunier, V.; Valeev, E. F.; Lampkins, A. J.; Li, H.; Castellano, R. K. A New Class of Supramolecular Wires. *J. Phys. Chem. C* **2007**, *111* (51), 18912−18916.

(20) Baker, M. B.; Yuan, L.; Marth, C. J.; Li, Y.; Castellano, R. K. Rapid access to C_3- and C_s-symmetric AAT organogelators via ring opening of a common benzotrifuranone precursor. *Supramol. Chem.* **2010**, *22* (11−12), 789−802.

(21) Yuan, L.; Sumpter, B. G.; Abboud, K. A.; Castellano, R. K. Links between through-bond interactions and assembly structure in simple piperidones. *New J. Chem.* **2008**, *32* (11), 1924−1934.
(22) Fagnani, D. E.; Meese, M. J., Jr.; Abboud, K. A.; Castellano, R. K. Homochiral [2.2]Paracyclophane Self-Assembly Promoted by Transannular Hydrogen Bonding. *Angew. Chem., Int. Ed.* **2016**, *55* (36), 10726−10731.
(23) Henderson, W. R.; Fagnani, D. E.; Grolms, J.; Abboud, K. A.; Castellano, R. K. Transannular Hydrogen Bonding in Planar-Chiral [2.2]Paracyclophane-Bisamides. *Helv. Chim. Acta* **2019**, *102* (4), No. e1900047.
(24) Korlepara, D. B.; Henderson, W. R.; Castellano, R. K.; Balasubramanian, S. Differentiating the mechanism of self-assembly in supramolecular polymers through computation. *Chem. Commun.* **2019**, *55* (26), 3773−3776.
(25) Henderson, W. R.; Zhu, Y.; Fagnani, D. E.; Liu, G.; Abboud, K. A.; Castellano, R. K. Self-Assembling [n.n]Paracyclophanes: A Structure-Property Relationship Study. *J. Org. Chem.* **2020**, *85* (2), 1158−1167.
(26) Henderson, W. R.; Kumar, A.; Abboud, K. A.; Castellano, R. K. Influence of Amide Connectivity on the Hydrogen-Bond-Directed Self-Assembly of [n.n]Paracyclophanes. *Chem. - Eur. J.* **2020**, *26* (72), 17588−17597.
(27) Henderson, W. R.; Castellano, R. K. Supramolecular polymerization of chiral molecules devoid of chiral centers. *Polym. Int.* **2021**, *70* (7), 897−910.
(28) Mayoral, M. J.; Guilleme, J.; Calbo, J.; Aragó, J.; Aparicio, F.; Ortí, E.; Torres, T.; González-Rodríguez, D. Dual-Mode Chiral Self-Assembly of Cone-Shaped Subphthalocyanine Aromatics. *J. Am. Chem. Soc.* **2020**, *142* (50), 21017−21031.
(29) Ueda, M.; Aoki, T.; Akiyama, T.; Nakamuro, T.; Yamashita, K.; Yanagisawa, H.; Nureki, O.; Kikkawa, M.; Nakamura, E.; Aida, T.; Itoh, Y. Alternating Heterochiral Supramolecular Copolymerization. *J. Am. Chem. Soc.* **2021**, *143* (13), 5121−5126.
(30) Chen, Y. T.; Baldridge, K. K.; Ho, D. M.; Pascal, R. A. Interconversion and Reactions of In- and Out-Isomers of a Triarylphosphine-Containing Cyclophane. *J. Am. Chem. Soc.* **1999**, *121* (51), 12082−12087.
(31) Qin, Q.; Mague, J. T.; Pascal, R. A. An in-Ketocyclophane. *Org. Lett.* **2010**, *12* (5), 928−930.
(32) Mannancherry, R.; Solomek, T.; Cavalli, D.; Malincik, J.; Haussinger, D.; Prescimone, A.; Mayor, M. Sulfone "Geländer" Helices: Revealing Unexpected Parameters Controlling the Enantiomerization Process. *J. Org. Chem.* **2021**, *86* (8), 5431−5442.
(33) Bachrach, S. M. DFT Study of [2.2]-, [3.3]-, and [4.4]-Paracyclophanes: Strain Energy, Conformations, and Rotational Barriers. *J. Phys. Chem. A* **2011**, *115* (11), 2396−2401.
(34) Dodziuk, H.; Szymański, S.; Jaźwiński, J.; Marchwiany, M. E.; Hopf, H. Structure and Dynamics of [3.3]Paracyclophane As Studied by Nuclear Magnetic Resonance and Density Functional Theory Calculations. *J. Phys. Chem. A* **2010**, *114* (38), 10467−10473.
(35) Dodziuk, H.; Szymański, S.; Jaźwiński, J.; Ostrowski, M.; Demissie, T. B.; Ruud, K.; Kuś, P.; Hopf, H.; Lin, S.-T. Structure and NMR Spectra of Some [2.2]Paracyclophanes. The Dilemma of [2.2]Paracyclophane Symmetry. *J. Phys. Chem. A* **2011**, *115* (38), 10638−10649.
(36) Szymański, S.; Dodziuk, H.; Pietrzak, M.; Jaźwiński, J.; Demissie, T. B.; Hopf, H. Dynamics of [n.3]paracyclophanes (n = 2 - 4) as studied by NMR. Obtaining separate Arrhenius parameters for two dynamic processes in [4.3]paracyclophane. *J. Phys. Org. Chem.* **2013**, *26* (7), 596−600.
(37) Demissie, T. B.; Dodziuk, H.; Waluk, J.; Ruud, K.; Pietrzak, M.; Vetokhina, V.; Szymański, S.; Jaźwiński, J.; Hopf, H. Structure, NMR and Electronic Spectra of [*m.n*]Paracyclophanes with Varying Bridges Lengths (*m*, *n* = 2−4). *J. Phys. Chem. A* **2016**, *120* (5), 724−736.
(38) Sato, T.; Wakabayashi, M.; Kainosho, M.; Hat, K. Conformational changes in the sulfur analogs of 11- and 12-membered metacyclophanes. *Tetrahedron Lett.* **1968**, *9* (39), 4185−4189.
(39) Boekelheide, V.; Mondt, J. L. An alternate synthesis of 2,11-dithia[3.3]metacyclophanes. *Tetrahedron Lett.* **1970**, *11* (14), 1203−1206.
(40) Krois, D.; Lehner, H. Conformational analysis—XIII: *Syn* and *anti* [3.2]-, [3.3]-, [4.2]-, and [4.3]-metacyclophanes. *Tetrahedron* **1982**, *38* (22), 3319−3324.
(41) Semmelhack, M. F.; Harrison, J. J.; Young, D. C.; Gutierrez, A.; Rafii, S.; Clardy, J. [3.3]Metacyclophane: a novel synthesis and a study of the structure through x-ray diffraction, molecular mechanics, and solution NMR analysis. *J. Am. Chem. Soc.* **1985**, *107* (25), 7508−7514.
(42) Sako, K.; Shinmyozu, T.; Takemura, H.; Suenaga, M.; Inazu, T. Conformational analysis of [3.3]cyclophanes. 4. A conformational study of [3.3]metacyclophanes through variable-temperature proton NMR and optical rotation. *J. Org. Chem.* **1992**, *57* (24), 6536−6541.
(43) Mitchell, R. H. Conformational Changes of 2,11-Dithia[3.3]-metacyclophane. A New Look Using VT NMR and Calculation. *J. Am. Chem. Soc.* **2002**, *124* (10), 2352−2357.
(44) Hayamizu, T.; Maeda, H.; Ouchi, T.; Kakiuchi, N.; Mizuno, K. Synthesis and Conformational Analysis of 2,11-Disila[3.3]-metacyclophanes. *Eur. J. Org. Chem.* **2016**, *2016* (23), 3934−3938.
(45) Maeda, H.; Endo, S.; Ouchi, T.; Mizuno, K.; Segi, M. Synthesis and Conformational Analysis of 2,11-Dioxa[3.3]metacyclophanes. *Chem. Lett.* **2017**, *46* (9), 1357−1360.
(46) Shieh, C.-F.; McNally, D.; Boyd, R. H. The heats of combustion and strain energies of some cyclophanes. *Tetrahedron* **1969**, *25* (17), 3653−3665.
(47) Givens, R. S.; Olsen, R. J.; Wylie, P. L. Mechanistic studies in photochemistry. 21. Photoextrusion of sulfur dioxide: general route to [2.2]cyclophanes. *J. Org. Chem.* **1979**, *44* (10), 1608−1613.
(48) Shear, T. A.; Lin, F.; Zakharov, L. N.; Johnson, D. W. "Design of Experiments" as a Method to Optimize Dynamic Disulfide Assemblies: Cages and Functionalizable Macrocycles. *Angew. Chem., Int. Ed.* **2020**, *59* (4), 1496−1500.
(49) Ehrlich, S.; Moellmann, J.; Grimme, S. Dispersion-Corrected Density Functional Theory for Aromatic Interactions in Complex Systems. *Acc. Chem. Res.* **2013**, *46* (4), 916−926.
(50) Anet, F. A. L.; Brown, M. A. Nuclear magnetic resonance studies of conformation and ring inversion in the [3.3]paracyclophane system. *J. Am. Chem. Soc.* **1969**, *91* (9), 2389−2391.
(51) Sako, K.; Meno, T.; Shinmyozu, T.; Inazu, T.; Takemura, H. Conformational Analysis of [3.3]Paracyclophane. *Chem. Ber.* **1990**, *123* (3), 639−642.
(52) Vogtle, F. Steric Interactions Inside Cyclic Compounds. 15. Dithia-Paracyclophane. *Chem. Zeit.* **1970**, *94* (9), 313.
(53) Bartlett, G. J.; Newberry, R. W.; VanVeller, B.; Raines, R. T.; Woolfson, D. N. Interplay of Hydrogen Bonds and n→π* Interactions in Proteins. *J. Am. Chem. Soc.* **2013**, *135* (49), 18682−18688.
(54) Choudhary, A.; Pua, K. H.; Raines, R. T. Quantum mechanical origin of the conformational preferences of 4-thiaproline and its *S*-oxides. *Amino Acids* **2011**, *41* (1), 181−186.
(55) Bürgi, H. B.; Dunitz, J. D.; Shefter, E. Geometrical reaction coordinates. II. Nucleophilic addition to a carbonyl group. *J. Am. Chem. Soc.* **1973**, *95* (15), 5065−5067.
(56) Bürgi, H. B.; Dunitz, J. D.; Lehn, J. M.; Wipff, G. Stereochemistry of reaction paths at carbonyl centres. *Tetrahedron* **1974**, *30* (12), 1563−1572.
(57) Staab, H. A.; Wahl, P.; Kay, K.-Y. Electron Donor-Acceptor Compounds, 45 Syntheses of [2.2]-, [3.3]-, and [4.4]Paracyclophanes with 1,2,4,5-Tetracyanobenzene Units as Electron Acceptors. *Chem. Ber.* **1987**, *120* (4), 541−549.
(58) Ernst, L.; Ibrom, K. ^{1}H, ^{13}C and ^{19}F NMR study of *ar*, *ar'*-difluoro[2.2]paracyclophanes, *ar*, *ar'*-difluoro-2,11-dithia[3.3]-paracyclophanes and their monofluoro analogues. Long-range ^{19}F,^{19}F spin-spin coupling. *Magn. Reson. Chem.* **1997**, *35* (12), 868−876.
(59) Wang, W.-L.; Xu, J.; Sun, Z.; Zhang, X.; Lu, Y.; Lai, Y.-H. Effect of Transannular π-π Interaction on Emission Spectral Shift and

https://doi.org/10.1021/jacs.1c05522
J. Am. Chem. Soc. XXXX, XXX, XXX−XXX

Fluorescence Quenching in Dithia[3.3]paracyclophane-Fluorene Copolymers. *Macromolecules* **2006**, *39* (21), 7277−7285.
(60) Xia, J.-L.; Zhang, C.; Zhu, X.; Ou, Y.; Jin, G.-J.; Yu, G.-a.; Liu, S. H. Substituted diethynyldithia[3.3]paracyclophanes—synthetically more accessible new building blocks for molecular scaffolding. *New J. Chem.* **2011**, *35* (1), 97−102.
(61) Yu, C.-Y.; Helliwell, M.; Raftery, J.; Turner, M. L. Synthesis and Ring-Opening Metathesis of Tetraalkoxy-Substituted [2.2]-Paracyclophane-1,9-dienes. *Chem. - Eur. J.* **2011**, *17* (25), 6991−6997.
(62) Auffray, M.; Kim, D. H.; Kim, J. U.; Bencheikh, F.; Kreher, D.; Zhang, Q.; D'Aléo, A.; Ribierre, J.-C.; Mathevet, F.; Adachi, C. Dithia[3.3]paracyclophane Core: A Versatile Platform for Triplet State Fine-Tuning and Through-Space TADF Emission. *Chem. - Asian J.* **2019**, *14* (11), 1921−1925.
(63) Staab, H. A.; Reimann-Haas, R.; Ulrich, P.; Krieger, C. Elektron-Donor-Acceptor-Verbindungen, XXX. Elektron-Donor-Acceptor-[2.2]Paracyclophane mit *N*,*N*,*N*′,*N*′-Tetramethyl-*p*-phenylendiamin (TMPD) als Donor-Einheit. *Chem. Ber.* **1983**, *116* (8), 2808−2826.
(64) Otsubo, T.; Boekelheide, V. An alternate route for the conversion of dithia[3.3]cyclophanes to cyclophane-dienes. Reaction with benzyne followed by sulfoxide pyrolysis. *Tetrahedron Lett.* **1975**, *16* (45), 3881−3884.
(65) Rebafka, W.; Staab, H. A. The Pseudogeminal "Quinhydrone" of the [2.2] Paracyclophane Series. *Angew. Chem., Int. Ed. Engl.* **1974**, *13* (3), 203−204.
(66) Staab, H. A.; Herz, C. P. Diastereomere [3.3]Paracyclophan-Chinhydrone. *Angew. Chem.* **1977**, *89* (11), 839−840.
(67) Mitchell, R. H.; Vinod, T. K.; Bodwell, G. J.; Bushnell, G. W. Preparation and NMR properties of tricarbonylchromium(0) derivatives of dithiacyclophanes. An estimate of the reduction in ring current of an aromatic ring on tricarbonylchromium complexation. *J. Org. Chem.* **1989**, *54* (25), 5871−5879.
(68) Montanari, M.; Bugana, A.; Sharma, A. K.; Pasini, D. Mild preparation of functionalized [2.2]paracyclophanes via the Pummerer rearrangement. *Org. Biomol. Chem.* **2011**, *9* (14), 5018−5020.
(69) Kattnig, D. R.; Mladenova, B.; Grampp, G.; Kaiser, C.; Heckmann, A.; Lambert, C. Electron Paramagnetic Resonance Spectroscopy of Bis(triarylamine) Paracyclophanes as Model Compounds for the Intermolecular Charge-Transfer in Solid State Materials for Optoelectronic Applications. *J. Phys. Chem. C* **2009**, *113* (7), 2983−2995.
(70) Kaiser, C.; Schmiedel, A.; Holzapfel, M.; Lambert, C. Long-Lived Singlet and Triplet Charge Separated States in Small Cyclophane-Bridged Triarylamine-Naphthalene Diimide Dyads. *J. Phys. Chem. C* **2012**, *116* (29), 15265−15280.
(71) Mladenova, B.; Kattnig, D. R.; Kaiser, C.; Schäfer, J.; Lambert, C.; Grampp, G. Investigations of the Degenerate Intramolecular Charge Exchange in Symmetric Organic Mixed Valence Compounds: Solvent Dynamics of Bis(triarylamine)paracyclophane Redox Systems. *J. Phys. Chem. C* **2015**, *119* (16), 8547−8553.
(72) Bléger, D.; Mathevet, F.; Kreher, D.; Attias, A.-J.; Bocheux, A.; Latil, S.; Douillard, L.; Fiorini-Debuisschert, C.; Charra, F. Janus-Like 3D Tectons: Self-Assembled 2D Arrays of Functional Units at a Defined Distance from the Substrate. *Angew. Chem., Int. Ed.* **2011**, *50* (29), 6562−6566.
(73) Bléger, D.; Kreher, D.; Mathevet, F.; Attias, A.-J.; Arfaoui, I.; Metgé, G.; Douillard, L.; Fiorini-Debuisschert, C.; Charra, F. Periodic Positioning of Multilayered [2.2]Paracyclophane-Based Nanopillars. *Angew. Chem., Int. Ed.* **2008**, *47* (44), 8412−8415.
(74) Gray, R.; Boekelheide, V. A study of the synthesis and properties of [2.2.2.2](1,2,4,5)cyclophane. *J. Am. Chem. Soc.* **1979**, *101* (8), 2128−2136.
(75) Ngola, S. M.; Kearney, P. C.; Mecozzi, S.; Russell, K.; Dougherty, D. A. A Selective Receptor for Arginine Derivatives in Aqueous Media. Energetic Consequences of Salt Bridges That Are Highly Exposed to Water. *J. Am. Chem. Soc.* **1999**, *121* (6), 1192−1201.
(76) Xu, J.; Wang, W.-L.; Lin, T.; Sun, Z.; Lai, Y.-H. Molecular assembly of dithiaparacyclophanes mediated by non-covalent X···X, X···Y and C-H···X (X, Y = Br, S, N) interactions. *Supramol. Chem.* **2008**, *20* (8), 723−730.
(77) Choudhary, A.; Gandla, D.; Krow, G. R.; Raines, R. T. Nature of Amide Carbonyl-Carbonyl Interactions in Proteins. *J. Am. Chem. Soc.* **2009**, *131* (21), 7244−7246.
(78) Sato, K.; Itoh, Y.; Aida, T. Homochiral supramolecular polymerization of bowl-shaped chiral macrocycles in solution. *Chem. Sci.* **2014**, *5* (1), 136−140.

https://doi.org/10.1021/jacs.1c05522
J. Am. Chem. Soc. XXXX, XXX, XXX−XXX